

Effect of tensor force on $2\nu\beta\beta$ and $0\nu\beta\beta$ decays in ^{76}Ge , ^{82}Se , ^{130}Te , and $^{136}\text{Xe}^*$

M.D. Wu (吴明德)¹ C.L. Bai (白春林)^{1†} D.L. Fang (房栋梁)^{2,3‡} Y.F. Niu (牛一斐)^{4,5}
H. Sagawa^{6,7} H.Q. Zhang (张焕乔)⁸

¹College of Physics, Sichuan University, Chengdu 610065, China

²Institute of Modern Physics, Chinese Academy of Sciences, Lanzhou 730000, China

³School of Nuclear Science, University of Chinese Academy of Sciences, Beijing 100049, China

⁴School of Nuclear Science and Technology, Lanzhou University, Lanzhou 730000, China

⁵Frontiers Science Center for Rare isotopes, Lanzhou University, Lanzhou 730000, China

⁶RIKEN Nishina Center for Accelerator-based Science, Wako 351-0198, Japan

⁷Center for Mathematics and Physics, University of Aizu, Aizu-Wakamatsu, Fukushima 965-8560, Japan

⁸China Institute of Atomic Energy, Beijing 102413, China

Abstract: The effects of the tensor force on the $2\nu\beta\beta$ and $0\nu\beta\beta$ decay nuclear matrix elements (NMEs) of ^{76}Ge , ^{82}Se , ^{130}Te , and ^{136}Xe are studied using the Hartree-Fock-Bogoliubov (HFB) plus proton-neutron quasi-particle random phase approximation (pnQRPA) model based on the Skyrme energy density functional. We include the full spectra of intermediate states with $J^\pi = 0^\pm \sim 10^\pm$ up to the energy cutoff $E = 60$ MeV, which is sufficient for convergence of NME calculations. The isovector (IV) pairing and tensor interactions are considered in both HFB and QRPA calculations, while the isoscalar (IS) pairing interaction is included only in QRPA calculations. We found that the tensor force shifts Gamow-Teller (GT) transition strengths substantially to low-energy regions and enhances the $2\nu\beta\beta$ decay NME. The inclusion of tensor force enhances the $0\nu\beta\beta$ NME by approximately 13% for ^{76}Ge and ^{82}Se and 30% for ^{130}Te and ^{136}Xe , for a fixed IS pairing strength. We found that the intermediate 2^- state makes an important contribution to the $0\nu\beta\beta$ NME, which is slightly enhanced by the inclusion of the tensor force. We also found that the contribution of the 1^+ state makes important differences through the inclusion of the tensor force, which enhances the contribution largely. However when the IS pairing strength is increased, the contributions from 1^+ states are rapidly reduced to be very small, resulting in even negative contributions. Thus, tensor and IS pairing effects cancel each other, making the net effect on the NME relatively small. Due to this cancellation, if the IS pairing strength is optimized separately for cases with and without the tensor interaction to reproduce the experimental $2\nu\beta\beta$ NME, the consequent $0\nu\beta\beta$ NME with the tensor interaction is close to that without the tensor interaction within a 10% difference.

Keywords: double beta decay, quasi-particle random phase approximation, tensor force, isoscalar pairing interaction

DOI: 10.1088/1674-1137/adcf8f **CSTR:** 32044.14.ChinesePhysicsC.49074112

I. INTRODUCTION

Double beta decay ($\beta\beta$ decay) is one of the most active topics in nuclear and particle physics [1, 2]. There are two types of $\beta\beta$ decay: two neutrino $\beta\beta$ decay ($2\nu\beta\beta$ decay) and zero neutrino $\beta\beta$ decay ($0\nu\beta\beta$ decay). The $0\nu\beta\beta$ decay is predicted by the nature of the Majorana neutrino hypothesis, where the neutrino is identical to the anti-

neutrino. Experimental observations of the $0\nu\beta\beta$ decay will justify the existence of Majorana neutrinos and provide important information on new physics beyond the standard model.

The $2\nu\beta\beta$ decay has been detected for decades [3], but the $0\nu\beta\beta$ decay has no experimental evidence so far, as the $0\nu\beta\beta$ decay may have an extremely long half-life, longer than the age of our universe. Precise prediction of

Received 27 January 2025; Accepted 23 April 2025; Published online 24 April 2025

* Supported by the National Natural Science Foundation of China (11575120, 11822504, 12075104) and National Key Research and Development (R&D) programme of China (2021YFA1601500). Science Specialty Program of Sichuan University (2020SCUNL210). D.L. Fang would like to acknowledge the support from Chinese Academy of Sciences for the project of Young Scientists in Basic Research (YSBR-099) and "From 0 to 1 innovative" program. This work was partially supported by JSPS KAKENHI (JP19K03858)

[†] E-mail: bclphy@scu.edu.cn

[‡] E-mail: dlfang@impcas.ac.cn

©2025 Chinese Physical Society and the Institute of High Energy Physics of the Chinese Academy of Sciences and the Institute of Modern Physics of the Chinese Academy of Sciences and IOP Publishing Ltd. All rights, including for text and data mining, AI training, and similar technologies, are reserved.

the half-life is essential for designing experimental facilities to detect this decay. Accurate simulations require knowledge of the neutrino mass term, the phase space factor, and the nuclear matrix element (NME) of decaying nuclei. While the phase space factor can be evaluated with high accuracy [4, 5], the NME still has a large variety depending on nuclear many-body models and also adopted effective interactions.

Several many-body methods have been adopted to calculate the $0\nu\beta\beta$ NME, see for examples the recent reviews [6–8]. In these models, the so-called closure approximation is often adopted without the explicit inclusion of excited states of intermediate odd-odd nuclei. In contrast, the quasi-particle random phase approximation (QRPA) has been applied extensively to study the $\beta\beta$ decay processes, without adopting the closure approximation [9–16].

In recent decades, the self-consistent spherical QRPA model have been applied to study the $\beta\beta$ decays [17–23], with emphasis on the overlap factor, IS pairing interaction, the paths of calculation. $\beta\beta$ decay is direct a decay, but QRPA calculations are done through a virtual processes, both $(Z, N) \rightarrow (Z, N-2) \rightarrow (Z+2, N-2)$ and $(Z, N) \rightarrow (Z+1, N-1) \rightarrow (Z+2, N-2)$ are different calculations paths. The axially symmetric deformations is taken into account in Refs. [24, 25]. A highly efficient finite amplitude method QRPA model incorporating axially symmetric deformation and large model spaces was developed to calculate the $2\nu\beta\beta$ decay in Ref. [26]. However, these calculations considered the central and spin-orbit components of the effective interactions, and the effects of the tensor force have not been explored.

As an important component of nucleon-nucleon interaction, the tensor force plays an important role in the evolution of nuclear shell structure [27–30], the nuclear collective excitations [31–35] such as the charge-exchange Gamow-Teller (GT) and spin-dipole (SD) transitions, and the relevant single beta decay half-lives [36, 37]. As the $\beta\beta$ decay is closely related to the charge-exchange excitations, it is of interest to explore the effect of tensor force on the $\beta\beta$ decay. In this study, the $2\nu\beta\beta$ and $0\nu\beta\beta$ NMEs, $M^{2\nu}$ and $M^{0\nu}$, of ^{76}Ge , ^{82}Se , ^{136}Xe , and ^{130}Te are investigated using the HFB+QRPA model based on the Skyrme energy density function (EDF) with the tensor force.

We briefly outline the theoretical framework and calculation details in Sec. II. In Sec. III, we present the effects of the tensor force on $M^{2\nu}$ and $M^{0\nu}$ and discuss the low-energy GT states. A summary is provided in Sec. IV.

II. FORMALISM

The $\beta\beta$ decays occur between the even-even nuclei, in which the initial and final states are denoted by 0_i^+ and 0_f^+ , respectively. It is a second-order weak process from

the initial to the final nuclei through virtual states of the intermediate odd-odd nucleus. Throughout this study, we assume that the $0\nu\beta\beta$ decay exists, and that the light neutrino-exchange mechanism dominates. The half-lives of the $2\nu\beta\beta$ decay and $0\nu\beta\beta$ decay can be expressed separately as [38, 39]

$$[T_{1/2}^{2\nu}(0_i^+ \rightarrow 0_f^+)]^{-1} = G^{(2\nu)}(0_f^+) \left| M_{\text{GT}}^{(2\nu)} \right|^2, \quad (1)$$

$$[T_{1/2}^{0\nu}]^{-1} = G^{(0\nu)} \left| M^{(0\nu)} \right|^2 \left(\frac{\langle m_{\beta\beta} \rangle}{m_e} \right)^2, \quad (2)$$

where $G^{(2\nu)}(0_f^+)$ and $G^{(0\nu)}$ are the phase space factors accounting for the outgoing leptons, and $\langle m_{\beta\beta} \rangle$ is the effective neutrino mass.

For the $2\nu\beta\beta$ decay NME, because of isospin symmetry, Fermi transition is highly suppressed so that only the NME of the GT transition, $M_{\text{GT}}^{2\nu}$, is considered in calculations. The GT NME, in the QRPA approach is expressed as [40]

$$M_{\text{GT}}^{2\nu} = \sum_{\mu\nu} \frac{\langle 0_f^+ \| O_{\text{GT}}^{(-)} \| 1_{\mu}^+ \rangle \langle 1_{\mu}^+ \| 1_{\nu}^+ \rangle \langle 1_{\nu}^+ \| O_{\text{GT}}^{(-)} \| 0_i^+ \rangle}{\frac{1}{2}[\omega_{\mu} + \omega_{\nu}]}, \quad (3)$$

where 1_{ν}^+ and 1_{μ}^+ are two sets of 1^+ intermediate states constructed on the ground states of the initial and final nuclei, respectively, using the QRPA method. In QRPA calculations, the HFB ground states are set as the initial (0_i^+) and final states (0_f^+). The energies ω_{ν} and ω_{μ} in the denominator correspond to the excitation energies relative to the ground states of initial and final nuclei [38]. In Eq. (3),

$$O_{\text{GT}}^{(\pm)} = \sum_i \sigma_i t_i^{(\pm)}, \quad (4)$$

which is the Gamow-Teller transition operator. The GT transition matrix element for QRPA can be expressed as

$$\langle 1_{\nu}^+ \| O_{\text{GT}}^{(-)} \| 0_i^+ \rangle = - \sum_{pn} \langle p \| \sigma \| n \rangle (X_{pn}^{iv} u_p v_n + Y_{pn}^{iv} v_p u_n), \quad (5)$$

$$\begin{aligned} \langle 0_f^+ \| O_{\text{GT}}^{(-)} \| 1_{\mu}^+ \rangle &= \langle 1_{\mu}^+ \| O_{\text{GT}}^{(+)} \| 0_f^+ \rangle \\ &= \sum_{pn} \langle n \| \sigma \| p \rangle (X_{pn}^{f\mu} u_n v_p + Y_{pn}^{f\mu} v_n u_p). \end{aligned} \quad (6)$$

The overlap factor in Eq. (3) is evaluated as [40]

$$\langle 1_{\mu}^+ | 1_{\nu}^+ \rangle = \mathcal{N} \sum_{p,n,p',n'} (X_{pn}^{iv} X_{p'n'}^{f\mu} - Y_{pn}^{iv} Y_{p'n'}^{f\mu}) \langle p | p' \rangle \langle n | n' \rangle. \quad (7)$$

In the above expressions, X and Y are the forward and

backward amplitudes of the QRPA states, and u and v are the unoccupation and occupation amplitudes of the HFB single-particle states in canonical basis [41]. The overlap of two single-particle states in the canonical basis can be expressed as

$$\langle k|k'\rangle = \delta_{ik,jk'} \delta_{jk,jk'} (u_k u_{k'} + v_k v_{k'}) \int_0^\infty u_k(r) u_{k'}(r) dr. \quad (8)$$

\mathcal{N} is the overlap factor between the initial and final ground states, calculated in the canonical basis using the approach introduced in Ref. [40].

The $0\nu\beta\beta$ NME, $M^{0\nu}$, is usually presented as a sum of three parts of two-body currents, GT, Fermi (FM), and Tensor (T) NMEs, expressed in the following separable form:

$$M^{0\nu} = M_{\text{GT}}^{0\nu} - \left(\frac{g_V}{g_A}\right)^2 M_{\text{F}}^{0\nu} + M_{\text{T}}^{0\nu}, \quad (9)$$

where g_V is the vector constant, and g_A is considered to be the same as $g_A^{\text{eff}} = 1.0$, consistent with the $2\nu\beta\beta$ NME calculations. Since the tensor term $M_{\text{T}}^{0\nu}$ is negligibly small [39], we calculate only the GT and Fermi terms:

$$\begin{aligned} M_{\text{F}}^{0\nu} &= \sum_k \langle 0_f^+ \| h_{\text{F}}(r_{12}, E_k) t_1^- t_2^- \| 0_i^+ \rangle, \\ M_{\text{GT}}^{0\nu} &= \sum_k \langle 0_f^+ \| h_{\text{GT}}(r_{12}, E_k) (\sigma_1 \cdot \sigma_2) t_1^- t_2^- \| 0_i^+ \rangle, \end{aligned} \quad (10)$$

where $r_{12} = |\mathbf{r}_1 - \mathbf{r}_2|$ is the relative coordinates of the two nucleons. The neutrino potential reads

$$h_{\text{K}}(r_{12}, E_k) = \frac{2R}{\pi} \int dq \frac{q h_{\text{K}}(q^2)}{q + E_k - (M_i + M_f)/2} j_0(qr_{12}), \quad (11)$$

where K denotes Fermi or GT, and R is the radius of the initial nuclei.

$j_0(qr_{12})$ is expanded as

$$j_0(qr_{12}) = 4\pi \sum_{lm} j_l(qr_1) j_l(qr_2) Y_{lm}^*(\Omega_1) Y_{lm}(\Omega_2), \quad (12)$$

and the NME can be written as

$$\begin{aligned} M_{\text{GT}}^{0\nu} &= 8R \int dq q h_{\text{GT}}(q^2) \sum_{k_1 k_2} \sum_{IJ} \frac{1}{2J+1} \\ &\times \frac{1}{q + (E_{k_1} + E_{k_2})/2 - (M_i + M_f)/2} \\ &\times [\langle J_{k_1} \| j_l(qr_1) (Y_l \otimes \sigma_1)^{(J)} t_1^+ \| 0_f^+ \rangle \langle J_{k_1} | J_{k_2} \rangle \\ &\times \langle J_{k_2} \| j_l(qr_2) (Y_l \otimes \sigma_2)^{(J)} t_2^- \| 0_i^+ \rangle], \end{aligned}$$

$$\begin{aligned} M_{\text{F}}^{0\nu} &= 8R \int dq q h_{\text{F}}(q^2) \sum_{k_1 k_2} \sum_{IJ} \frac{1}{2J+1} \\ &\times \frac{1}{q + (E_{k_1} + E_{k_2})/2 - (M_i + M_f)/2} \\ &\times [\langle J_{k_1} \| j_l(qr_1) Y_l t_1^+ \| 0_f^+ \rangle \langle J_{k_1} | J_{k_2} \rangle \\ &\times \langle J_{k_2} \| j_l(qr_2) Y_l t_2^- \| 0_i^+ \rangle], \end{aligned} \quad (13)$$

where J_{k_1} and J_{k_2} are the QRPA excited states with total angular momentum J , calculated from the ground states of the final and initial nuclei, respectively. Detailed expressions of $h_{\text{GT}}(q^2)$ and $h_{\text{F}}(q^2)$ are found in Ref. [39].

For the details of QRPA solutions and the Skyrme HFB, one could refer to [42, 43]. In this study, we adopt the volume pairing interaction, which is divided into IV and IS components:

$$V_q^{\text{IV}} = V_0^q \frac{1 - P_\sigma}{2} \delta(\mathbf{r}), \quad (14)$$

$$V^{\text{IS}} = f V_0 \frac{1 + P_\sigma}{2} \delta(\mathbf{r}), \quad (15)$$

where $\mathbf{r} = \mathbf{r}_1 - \mathbf{r}_2$ is the distance between the two nucleons, and P_σ is the spin exchange operator. The IV pairing is included in both HFB and QRPA calculations, and strength $V_0^q (q = n, p)$ is fixed in HFB calculation by empirical pairing gaps of the neutron and proton, respectively. The IS pairing interaction is included only in the pp channel of the QRPA equation, and the strength is decided by two factors, V_0 is the mean value of V_0^n and V_0^p , and f is a free parameter.

The Skyrme-type tensor interaction is adopted atop the central part of the EDF in our calculations, given by

$$\begin{aligned} V^T &= \frac{T}{2} \{[(\sigma_1 \cdot \mathbf{k}')(\sigma_2 \cdot \mathbf{k}) - \frac{1}{3}(\sigma_1 \cdot \sigma_2) \mathbf{k}'^2] \delta(\mathbf{r}) \\ &+ \delta(\mathbf{r}) [(\sigma_1 \cdot \mathbf{k})(\sigma_2 \cdot \mathbf{k}) - \frac{1}{3}(\sigma_1 \cdot \sigma_2) \mathbf{k}^2]\} \\ &+ \frac{U}{2} \{(\sigma_1 \cdot \mathbf{k}') \delta(\mathbf{r})(\sigma_2 \cdot \mathbf{k}) + (\sigma_2 \cdot \mathbf{k}') \delta(\mathbf{r})(\sigma_1 \cdot \mathbf{k}) \\ &- \frac{2}{3} [(\sigma_1 \cdot \sigma_2) \mathbf{k}' \cdot \delta(\mathbf{r}) \mathbf{k}]\}, \end{aligned} \quad (16)$$

where $\mathbf{k} = (\nabla_1 - \nabla_2)/2i$ acts on the right, and $\mathbf{k}' = -(\nabla_1' - \nabla_2')/2i$ acts on the left. The parameters T and U denote the strengths of triplet-even (TE) and triplet-odd (TO) tensor force, respectively. This type of tensor interactions was first presented by T. H. R. Skyrme in the 1950s [44, 45].

III. RESULTS

In $\beta\beta$ decay experiments, ^{76}Ge has been used in LE-

GEND [46] and CDEX [47], ^{82}Se will be used in NvDex [48], ^{136}Xe has been used in KamLAND-Zen collaboration [49], PandaX [50], EXO-200 [51] and NEXT [52], and ^{130}Te has been used in CUORE [53]. We perform self-consistent HFB+QRPA for the 2ν and $0\nu\beta\beta$ decays in ^{76}Ge , ^{82}Se , ^{130}Te and ^{136}Xe . The calculated results converge when the cutoff energy of the intermediate states is set to 60 MeV. In our calculations, the Skyrme interaction SGII is adopted [54], which gives a reasonable Landau-migdal parameter for the spin-isospin channel, $g'_0 = 0.498$, having the effective mass $m^*/m = 0.786$. The tensor interaction is included with $(T,U) = (500, -350)$ MeV $\cdot\text{fm}^5$, referred to as "Te1." This strength is optimized based on studies of the centroid energies of GT and charge-exchange spin-dipole (SD) giant resonances [55–58]. These studies yield reasonable descriptions of the low-lying 0^+ , 2^+ , and 3^- states, as well as the giant GT transitions within the subtracted second random phase approximation (SSRPA) [59, 60].

A. Nuclear matrix element $M_{\text{GT}}^{2\nu}$ for the $2\nu\beta\beta$ decay

The dependence of the $\beta\beta$ decay NME on IV and IS pairings has been well studied in QRPA [15, 24, 61]. These studies suggest that $M_{\text{GT}}^{2\nu}$ is influenced by the IS pairing but is not sensitive to the IV pairing [15, 61]. As the tensor force has strong effect on the low-lying GT transitions [31], it is valuable to study the effect of the tensor force on the $M_{\text{GT}}^{2\nu}$.

Before discussing the NME, we first present the overlap factors \mathcal{N} calculated with and without tensor force in Table 1. The average value of these overlap factors for open shell nuclei is approximately 0.8, consistent with

Table 1. Overlap factor \mathcal{N} between the initial and final ground states obtained using HFB calculations with the SGII+Te1 interaction, including (w/i) and excluding (w/o) the tensor force.

Nuclei	w/o	w/i
^{76}Ge	0.789	0.784
^{82}Se	0.780	0.773
^{130}Te	0.808	0.814
^{136}Xe	0.447	0.473

results obtained from deformed calculations [14, 16, 40]. The presence of tensor force does not largely affect this factor. For ^{136}Xe , a strong suppression for the overlap factor is observed due to the neutron magicity $N = 82$ of this nucleus. For this nucleus, we find that the tensor force changes this factor by more than 5%. This implies that, for magic nuclei, the tensor force may affect the structure of ground state. In contrast, it was suggested in Ref. [62] that such suppression for magic nuclei may be overestimated due to the particle number non-conservation nature of the HFB theory, and a larger overlap factor is expected when the number projection is applied to the calculation. To confirm this point, the number projected by the HFB theory is needed for further investigation.

Figure 1 shows the dependence of $M_{\text{GT}}^{2\nu}$ on the IS pairing strength and tensor force for ^{76}Ge , ^{82}Se , ^{130}Te , and ^{136}Xe . Two different curves are presented: one with ("w/i") and one without ("w/o") the tensor interaction in the HFB+QRPA calculations. Our results on the IS pairing strength dependence are consistent with the results of other QRPA studies [40, 64, 65]. The NME changes

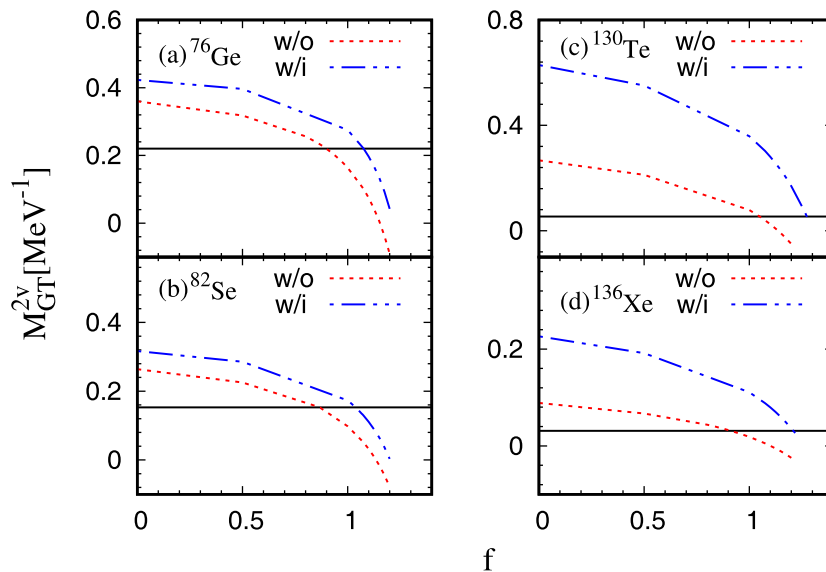


Fig. 1. (color online) $M_{\text{GT}}^{2\nu}$ values of ^{76}Ge , ^{82}Se , ^{130}Te and ^{136}Xe obtained by the HFB+QRPA calculation for different strengths of the IS pairing interaction. Results with (blue dash-dot-dot line) and without (red dotted line) the tensor interaction are labeled "w/i" and "w/o," respectively. The experimental value is shown as a black horizontal line [63].

smoothly when the IS pairing strength is small and then at a certain value of f close to the critical point, the NME starts to change drastically until the collapse of QRPA solutions. This general trend is not altered by including the tensor force.

For the NMEs of ^{76}Ge and ^{82}Se , as shown in Fig. 1(a) and (b), the results show that the tensor force enhances the NMEs notably. In ^{76}Ge and ^{82}Se , the tensor force increases the NMEs by approximately 20% when the IS pairing is absent. For ^{76}Ge , when we increase the strength of the IS pairing up to $f = 1.0$, the NME is enhanced by a constant amount of approximately 0.1 by the tensor force. Near the critical value $f = 1.1$, the NMEs drop rapidly for the cases without and with the tensor force $f = 1.1$, reaching 0.075 and 0.197, respectively. For ^{82}Se , the effect of tensor force is similar to the case of ^{76}Ge ; it increases the NME always by 0.05~0.07. When the value f is approaching to 1.1, the NME is enhanced even more by the tensor force, *i.e.*, the NME becomes 0.032 and 0.111 without and with the tensor force at $f = 1.1$, respectively. For ^{130}Te and ^{136}Xe , as shown in Fig. 1(c) and (d), the enhancement of the NMEs by the tensor force is much larger compared to that for ^{76}Ge and ^{82}Se . Without IS pairing, the NMEs increase by more than a factor 2. This enhancement continues even with a large IS pairing with $f = 1.0$. When the IS pairing is approaching $f = 1.1$, the NMEs of both ^{130}Te and ^{136}Xe are changed from negative to positive values by the tensor force.

The values of f that reproduce the experimental NMEs are listed in Table 2. As noted previously, these results confirm that the tensor force enhances the NME, and therefore, a larger f value is needed to reproduce the

measured NME.

The GT^- strength distributions in ^{76}Ge , ^{82}Se , ^{130}Te , and ^{136}Xe calculated using the IS pairing strengths listed in Table 2 with and without the tensor force are shown in Fig. 2. For ^{76}Ge as shown in the Fig. 2(a), the QRPA calculations give the three-peak structure observed also in the experimental data. Including the tensor force shifts the main peak energy downward by approximately 0.5 MeV and obtains an excitation energy approximately 1 MeV higher than that obtained via experiment. Increasing the IS pairing from f_1 to f_2 reduces the strengths in the giant GT^- resonances, which is the reason why the increasing of IS pairing rapidly reduces the $2\nu\beta\beta$ NME. In contrast, the inclusion of tensor force alters the excitation energies in both low and high energy region. For ^{82}Se as

Table 2. Values of IS pairing strength f to reproduce the experimental NMEs and the corresponding $M_{\text{GT}}^{2\nu}$. f_1 and f_2 are the optimized values without (w/o) and with (w/i) the tensor force, respectively.

Nuclei	$M_{\text{exp}}^{2\nu}$	Tensor	f_1 or f_2	$M_{\text{GT}}^{2\nu}$
^{76}Ge	0.220	w/o	$f_1 = 0.900$	0.219
		w/i	$f_2 = 1.075$	0.221
^{82}Se	0.153	w/o	$f_1 = 0.866$	0.153
		w/i	$f_2 = 1.038$	0.153
^{130}Te	0.054	w/o	$f_1 = 1.050$	0.054
		w/i	$f_2 = 1.274$	0.053
^{136}Xe	0.031	w/o	$f_1 = 0.920$	0.030
		w/i	$f_2 = 1.211$	0.030

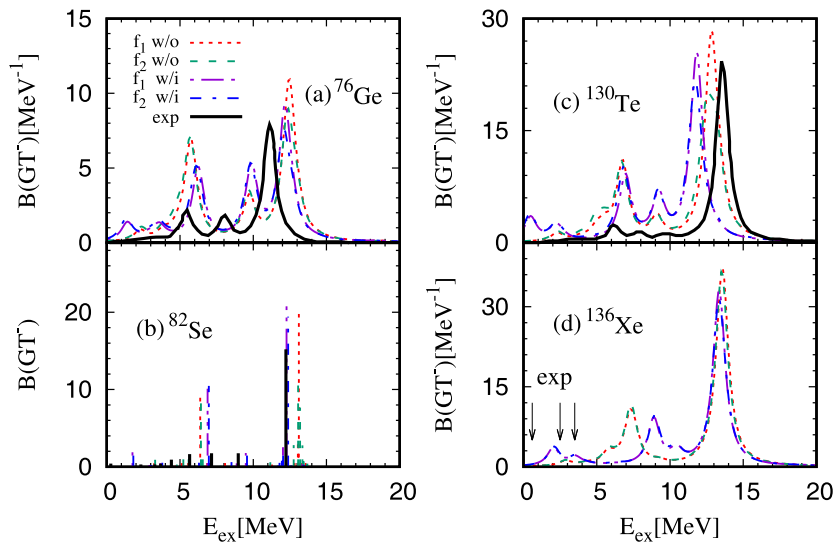


Fig. 2. (color online) GT^- transition strength function for ^{76}Ge , ^{82}Se , ^{130}Te , and ^{136}Xe . E_{ex} is the excitation energy of the final nuclei. The results obtained by the calculations with (f_1 -purple dash-dot-dot line, f_2 -blue dash-dot line) or without (f_1 -red dotted line, f_2 -green dashed line) tensor interaction are labeled by "w/i" or "w/o," respectively, and f_1 and f_2 are the IS pairing strengths. Experimental data are shown by black lines for ^{76}Ge and ^{130}Te , while the data are given by black horizontal lines for ^{82}Se [69, 70].

shown in panel (b), the main peak energy is approximately 1 MeV higher than the experimental data when the tensor force is absent. Including the tensor force shifts the peak downward by 1 MeV, achieving good agreement with the experimental data. For ^{130}Te , the main peak energy obtained with the tensor force is approximately 1.8 MeV lower than the experimental one, partly due to the strong IS pairing required to reproduce the NME. For ^{136}Xe , the calculation with the tensor force produces the low excitation energy distribution at approximately 2 MeV, which is consistent with experimental observations. The calculated main peak energies for the three nuclei ^{76}Ge , ^{82}Se , and ^{130}Te obtained with the inclusion of the tensor force are within a 2 MeV difference from the experimental data. This is reasonable since the strength of the tensor force was optimized to reproduce the main GT peak energies of doubly-closed shell nuclei within 2.5 MeV differences in Ref. [55]. For all four nuclei in Fig. 2, the inclusion of the tensor force shifts the main peak energies downward and enhances the strength of low-energy states, which may explain the enhancement of the NME owing to the tensor force.

For a more comprehensive understanding of the effect of the tensor force on $M_{\text{GT}}^{2\nu}$, we show in Fig. 3 the GT^{\pm} strength distributions for the initial and final nuclei ^{76}Ge and ^{76}Se as well as ^{130}Te and ^{130}Xe obtained with and without the tensor force without the pn pairing. Since the cases of ^{76}Ge and ^{130}Te are similar to ^{82}Se and ^{136}Xe respectively, ^{76}Ge and ^{130}Te are chosen as representatives to examine the tensor force effects on NMEs. For ^{76}Ge with the tensor force included as shown in panel (a), the lowest GT state is shifted downward by approximately 0.8 MeV. In contrast, for ^{76}Se as shown in panel (b), the excitation energy of the lowest GT^+ state is kept un-

changed. The strengths in the lowest states are enhanced by approximately a factor 2 by the inclusion of tensor force. These two effects of tensor force are the main reason that the tensor force obviously enhances the $M_{\text{GT}}^{2\nu}$ of ^{76}Ge . In contrast, for ^{130}Te and ^{130}Xe , as shown in panels (c) and (d), the lowest GT^- and GT^+ states shift downward by approximately 2.0 MeV and 0.8 MeV, respectively, with the tensor force. Moreover, the GT strengths in the lowest states are dramatically increased, particularly the GT^+ strength which is increased by approximately one order of magnitude. Consequently, a much stronger effect of tensor force on the NME of ^{130}Te is observed in Fig. 1.

To further clarify the effect of tensor force on the GT states, important configurations for ^{76}Ge , ^{76}Se , ^{130}Te , and ^{130}Xe are listed in Table 3. For ^{76}Ge and ^{76}Se , the most important configuration is $(\pi 2p_{3/2}, \nu 2p_{1/2})$, while it is $(\pi 2d_{5/2}, \nu 2d_{3/2})$ for ^{130}Te and ^{130}Xe . As reported in Ref. [27], the tensor force produces an attractive effect between protons and neutrons in the j_{\geq} and j_{\leq} orbits and a repulsive effect between protons and neutrons in j_{\geq} and j_{\geq} orbits. As a result, the tensor force shifts the lowest GT states downward. Some differences exist among the nuclei listed in the table. For ^{76}Ge and ^{76}Se , there are appreciable contributions from the $(\pi 2p_{1/2}, \nu 2p_{1/2})$ configuration after the tensor force is included, which cancels the attractive effect slightly. However, for ^{130}Te and ^{130}Xe all the important configurations experience the attractive effect of the tensor force. This is the reason that the effects of the tensor force are stronger in ^{130}Te and ^{136}Xe .

Recent $2\nu\beta\beta$ decay experiments provide detailed electron spectra that offer valuable information about contributions from states with different excitation energies. This information can be used to further constrain the nuc-

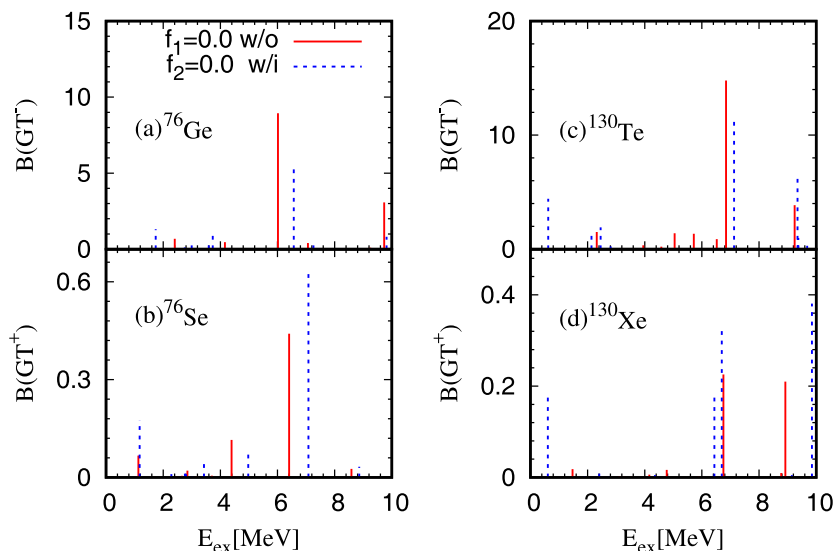
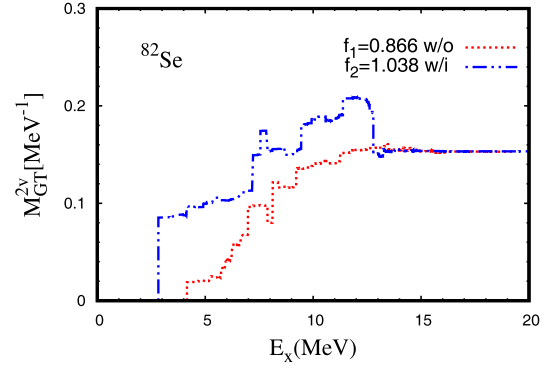


Fig. 3. (color online) GT^{\pm} strength distributions for the initial and final nuclei ^{76}Ge and ^{76}Se as well as ^{130}Te and ^{130}Xe obtained with pn pairing strength $f=0$ in cases with (blue dotted lines) and without (red solid lines) the tensor force.

Table 3. Important configurations in the lowest GT states of initial and final nuclei obtained with $f = 0.0$, in cases with and without the tensor force.

Nuclei	Tensor	E_{ex}	$B(\text{GT}\pm)$	Configuration	$\chi^2 - Y^2$
^{76}Ge	w/o	2.40	0.69	$(\pi 2p_{3/2}, \nu 2p_{1/2})$	0.948
				$(\pi 2p_{1/2}, \nu 2p_{3/2})$	0.016
				$(\pi 2p_{3/2}, \nu 2p_{3/2})$	0.022
	w/i	1.73	1.31	$(\pi 2p_{1/2}, \nu 2p_{1/2})$	0.045
				$(\pi 2p_{3/2}, \nu 2p_{1/2})$	0.895
				$(\pi 2p_{3/2}, \nu 1f_{5/2})$	0.052
^{76}Se	w/o	1.13	0.07	$(\pi 2p_{3/2}, \nu 2p_{1/2})$	0.964
				$(\pi 2p_{1/2}, \nu 2p_{3/2})$	0.015
				$(\pi 2p_{3/2}, \nu 2p_{3/2})$	0.011
	w/i	1.17	0.18	$(\pi 2p_{1/2}, \nu 2p_{1/2})$	0.089
				$(\pi 2p_{3/2}, \nu 2p_{1/2})$	0.887
				$(\pi 2p_{3/2}, \nu 1f_{5/2})$	0.016
^{130}Te	w/o	2.32	1.50	$(\pi 3s_{1/2}, \nu 3s_{1/2})$	0.010
				$(\pi 2d_{3/2}, \nu 2d_{3/2})$	0.006
				$(\pi 2d_{5/2}, \nu 2d_{3/2})$	0.925
	w/i	0.62	4.42	$(\pi 2d_{5/2}, \nu 2d_{5/2})$	0.022
				$(\pi 3s_{1/2}, \nu 2d_{3/2})$	0.046
				$(\pi 2d_{5/2}, \nu 2d_{3/2})$	0.883
^{130}Xe	w/o	1.47	0.02	$(\pi 2d_{5/2}, \nu 1g_{7/2})$	0.046
				$(\pi 3s_{1/2}, \nu 3s_{1/2})$	0.011
				$(\pi 2d_{3/2}, \nu 2d_{3/2})$	0.006
	w/i	0.61	0.19	$(\pi 2d_{5/2}, \nu 2d_{3/2})$	0.932
				$(\pi 2d_{5/2}, \nu 2d_{5/2})$	0.020
				$(\pi 3s_{1/2}, \nu 2d_{3/2})$	0.049
				$(\pi 2d_{5/2}, \nu 2d_{3/2})$	0.894
				$(\pi 2d_{5/2}, \nu 1g_{7/2})$	0.035

lear structure calculations beyond the NME [66]. The running sums of NMEs in ^{82}Se and ^{136}Xe are measured [67, 68]. However, the results for ^{136}Xe have large uncertainties and cannot uniquely determine the running sum yet [66]. For ^{82}Se , a strong preference to the single-state dominance (SSD) feature for the running sum is observed, *i.e.*, contribution from the lowest 1^+ state exhausts almost all of the total $M_{\text{GT}}^{2\nu}$. The running sums of $M_{\text{GT}}^{2\nu}$ for ^{82}Se are shown in Fig. 4. Without the tensor force, the running sum starts at approximately 0.02 and increases steadily up to a final value of approximately 0.15, with most contributions coming from high-lying states. When the tensor force is included, the running sum starts at approximately 0.08, which contributes more than 50% to the total $M_{\text{GT}}^{2\nu}$. This suggests that including the tensor force is necessary in NME calculations.

**Fig. 4.** (color online) Running sum of the NME $M_{\text{GT}}^{2\nu}$ in ^{82}Se as a function of the excitation energy E_x with the optimized IS pairing strength f_1 or f_2 . $E_x = (\omega_\mu + \omega_\nu)/2$ is the averaged excitation energy given in Eq. (3). Results obtained with (blue dash-dot-dot line) and without (red dotted line) the tensor interaction are labeled "w/i" or "w/o," respectively.

B. Nuclear matrix element $M^{0\nu}$ for the $0\nu\beta\beta$ decay

After the strength parameter f of IS pairing interaction is fixed by the $2\nu\beta\beta$ NME, we performed calculations of the $0\nu\beta\beta$ NMEs for ^{76}Ge , ^{82}Se , ^{130}Te , and ^{136}Xe . The calculations include intermediate states with J^π ranging from 0^\pm to 10^\pm .

The $M^{0\nu}$ values for ^{76}Ge , ^{82}Se , ^{130}Te , and ^{136}Xe calculated with different values of IS pairing strength factor f , with and without the tensor force, are shown in Fig. 5. As shown in Fig. 1, reproducing $M_{\text{GT}}^{2\nu}$ in the calculations with or without tensor force need different IS pairing strengths. In Fig. 5, the IS pairing strength factor fixed by $M_{\text{GT}}^{2\nu}$ in the calculations without and with the tensor force are labeled f_1 and f_2 , respectively. One can see from the figure that, when $M_{\text{GT}}^{2\nu}$ values are reproduced, including the tensor force brings small changes to $M^{0\nu}$, which is consistent with the results in Ref. [23]. However, for calculations using the same factor f , either including or excluding the tensor force (indicated by filled or empty symbols of the same shape), the inclusion of the tensor force leads to evident differences in the $M^{0\nu}$ values.

The relative change of $M^{0\nu}$ caused by the inclusion of the tensor force is shown in Fig. 6 as the ratio $(M_{\text{w/i}}^{0\nu}(f) - M_{\text{w/o}}^{0\nu}(f))/M_{\text{w/o}}^{0\nu}(f)$. For the fixed IS pairing strength f_1 or f_2 , the tensor force increases the ratio by approximately 13% for ^{76}Ge and ^{82}Se and approximately 30% for ^{130}Te and ^{136}Xe . However, the ratio $(M_{\text{w/i}}^{0\nu}(f_2) - M_{\text{w/o}}^{0\nu}(f_1))/M_{\text{w/o}}^{0\nu}(f_1)$ varies only slightly with the change in f factor from f_1 w/o the tensor to f_2 with the tensor; if the pairing strengths are optimized by the experimental $M_{\text{GT}}^{2\nu}$ with or without tensor force, the net results of IS pairing and tensor coupling for $M^{0\nu}$ cause only small changes, *i.e.*, approximately -3% for ^{76}Ge and ^{82}Se and -8.0% and -9.0% for ^{130}Te and ^{136}Xe , respectively, compared with

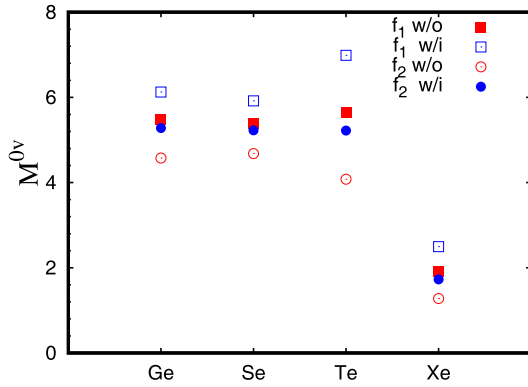


Fig. 5. (color online) $M^{0\nu}$ values for ^{76}Ge , ^{82}Se , ^{130}Te , and ^{136}Xe . The results obtained by the calculations with (blue) or without (red) the tensor interaction are labeled by "w/i" or "w/o," respectively.

those obtained with the optimized value f_1 without the tensor interaction. As noticed before, this is due to the fact that the inclusion of the tensor force requires a larger IS pairing so as to reproduce $M_{\text{GT}}^{2\nu}$, but the stronger IS pairing cancels the effect of the tensor force.

For more details, the contributions of all the intermediate states to $M^{0\nu}$ calculated with different f values f_1 and f_2 are displayed in Fig. 7. For each f value, we examine the effect of tensor interaction without introducing the closure approximation. Since the cases of ^{76}Ge and ^{130}Te are similar to ^{82}Se and ^{136}Xe respectively, ^{76}Ge and ^{130}Te are chosen as representatives to examine the interplay between IS pairing and tensor interactions. Both the tensor force and IS pairing interactions make small contributions to the NME through the state with $J > 2$. This is due to the exchange momentum q in the neutrino potential in Eq. (11); for larger J , larger q is needed to contribute to the matrix element of $j_i(qr)$. For ^{76}Ge , as shown in panels (a) and (b), or (c) and (d), when calculated with the fixed IS pairing strength factor f_1 or f_2 , the tensor force evidently increases NMEs through 1^+ and 2^- intermediate states. Consequently, including tensor force enhances the NME as can be seen in comparisons between panels (a) and (b) or between (c) and (d). While comparing panels (a) and (d), in which experimental $M_{\text{GT}}^{2\nu}$ values are reproduced by optimized IS pairing strengths, the larger IS pairing strength f_2 reduces the NME largely through 1^+ states, while the tensor interaction increases the contribution of 2^- states. Therefore, the effects of the tensor force and IS pairing on the NME largely cancel each other in panels (a) and (d).

In the case of ^{130}Te , comparisons between panels (e) and (f) or (g) and (h) of Fig. 7 show that including the tensor force substantially increases the NME through 1^+ and 2^- intermediate states, even more than that for ^{76}Ge . For the 2^- states, in calculations with both f_1 and f_2 cases, the tensor force slightly enhances the NME. In contrast, for 1^+ states, when increasing the IS pairing

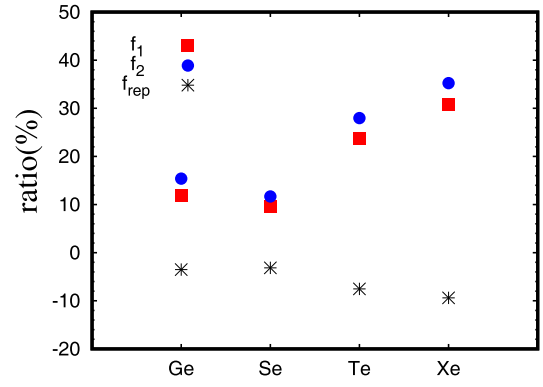


Fig. 6. (color online) Relative change of $M^{0\nu}$ caused by the inclusion of the tensor force. The ratio is defined by $\frac{M_{w/i}^{0\nu}(f) - M_{w/o}^{0\nu}(f)}{M_{w/o}^{0\nu}(f)}$, for ^{76}Ge , ^{82}Se , ^{130}Te , and ^{136}Xe . Results are labeled by the IS pairing strength f_1 or f_2 , while f_{rep} represents the ratio $\frac{M_{w/i}^{0\nu}(f_2) - M_{w/o}^{0\nu}(f_1)}{M_{w/o}^{0\nu}(f_1)}$.

strength from f_1 to f_2 , the contribution is reduced rapidly from the magnitude similar to that for 2^- states with f_1 to a very small value with f_2 , even negative in some cases. As a net effect, we can see that the inclusion of the tensor interaction enhances the contribution, but cancels largely the effect of IS pairing. Additionally, the stronger IS pairing f_2 reduces the NME, especially through 1^+ states, compared to the weaker IS pairing f_1 , as seen between panels (e) and (g) or (f) and (h).

The present results differ from those reported in Ref. [10] in which the 1^- states also make important contributions. This discrepancy may arise from differences in the single-particle states and residual interactions used in the calculations. Moreover in our calculations, the 1^- states are located at higher energies which reduce the contribution to the NME.

In this study, the $\beta\beta$ NMEs are investigated within the spherical approximation, although the initial and final nuclei of the four double β decay candidates may be deformed. It has been reported that NMEs are reduced when there is a significant difference in deformation between the initial and final nuclei [62], as the overlap factor between the two nuclei decreases with deformation difference. According to empirical results, similar deformations of the initial and final nuclei occur for ^{82}Se and ^{136}Xe , but evidently different values occur for ^{76}Ge and ^{130}Te . The $0\nu\beta\beta$ NMEs are studied by using Skyrme interaction with axial deformation in Ref. [24]. There, the $M^{0\nu}$ value for ^{76}Ge closely matches our results without the tensor force, reflecting the similar deformations of the initial and final nuclei. However, $M^{0\nu}$ values for ^{130}Te and ^{136}Xe are significantly suppressed due to the evidently different deformations in terms of absolute values or signs. Since the quadrupole deformation factor β_2 is not well reproduced in the HFB calculation even qualitatively, it is valuable to check the $\beta\beta$ NMEs with realistic

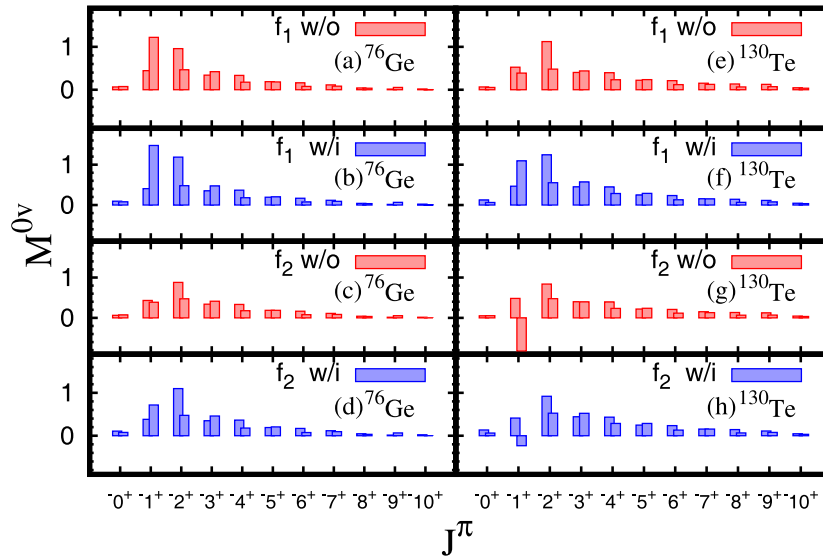


Fig. 7. (color online) $M^{0\nu}$ value of each J^π for ^{76}Ge and ^{130}Te at different f values with or without the tensor force; f_1 is determined by the experimental value obtained without (w/o) the tensor force (red rectangle), and f_2 is determined by the experimental value obtained with (w/i) the tensor force (blue rectangle).

deformations qualitatively and quantitatively in future work.

IV. SUMMARY

HFB+QRPA calculations employing the Skyrme interaction SGII were performed to study the $2\nu\beta\beta$ and $0\nu\beta\beta$ decay NMEs in ^{76}Ge , ^{82}Se , ^{130}Te , and ^{136}Xe taking into account the tensor interaction. Along with the tensor interaction, the IV pairing interaction was adopted in the HFB and QRPA calculations, while the IS pairing interaction was included only in the QRPA calculations. The $2\nu\beta\beta$ decay is dominated by intermediate 1^+ states, and the inclusion of the tensor force enhances $M_{\text{GT}}^{2\nu}$ largely because the tensor force shifts low energy GT states downward, increasing $M_{\text{GT}}^{2\nu}$. Consequently, a stronger IS pairing is required to reproduce the experimental $2\nu\beta\beta$ NMEs, $M_{\text{GT}}^{2\nu}$, when the tensor interaction is included, compared to the calculations without it. Specifically, the optimized IS strength f_1 is approximately 0.9 to 1.0 when the tensor force is absent, but the value f_2 becomes approximately 15% larger to be approximately 1.0 for ^{76}Ge and ^{82}Se and 1.2 for ^{130}Te and ^{136}Xe with the inclusion of the tensor force. Experimental $2\nu\beta\beta$ electron spectra for ^{82}Se indicate that the running sum is dominated by the lowest 1^+ state, and the calculated results are largely improved by the tensor interaction showing a substantially large contribution from the lowest 1^+ state.

The $0\nu\beta\beta$ NMEs, $M^{0\nu}$, were calculated including the full spectra of intermediate states with $J^\pi = 0^\pm \sim 10^\pm$ up to an energy cutoff $E = 60$ MeV, which is sufficient for convergence to calculate the NMEs without employing the closure approximation. In calculations with the fixed IS pairing strength, the inclusion of the tensor interaction enhances the NME by approximately 13% for ^{76}Ge and ^{82}Se and by approximately 30% for ^{130}Te and ^{136}Xe . However, when the IS pairing strengths are optimized to reproduce experimental $2\nu\beta\beta$ NME, denoted as f_1 or f_2 ($f_1 < f_2$), the tensor effect cancels the larger IS pairing effect, resulting in the net effect of the tensor and IS pairing interactions becoming smaller, *i.e.*, at most 10%. We found that the 2^- state makes an important contribution to $0\nu\beta\beta$ NME, which is affected by the tensor force. More attention should be given to the 1^+ state, as its contribution to the NME is strongly influenced by IS pairing and tensor interaction. Specifically, inclusion of the tensor force significantly enhances the contribution to the NME, but its contribution is reduced significantly by the IS pairing: the increase in IS pairing strength from f_1 to f_2 changes the contribution of the 1^+ states from a magnitude similar to 2^- state to a very small value, resulting in even a negative contribution. In other words, although the tensor force enhances contributions from both 1^+ and 2^- intermediate states to $M^{0\nu}$, the stronger IS pairing in the presence of the tensor force largely suppresses these low spin state contributions.

References

- [1] F. T. Avignone III, S. R. Elliott, and J. Engel, *Rev. Mod. Phys.* **80**, 481 (2008)
- [2] S. R. Elliott and M. Franz, *Rev. Mod. Phys.* **87**, 137 (2015)
- [3] M. Moe, *Ann. Rev. Nucl. Part. Sci.* **64**, 247 (2014)

- [4] J. Kotila and F. Iachello, *Phys. Rev. C* **85**, 034316 (2012)
- [5] M. Mirea, T. Pahomi, and S. Stoica, *Rom. Rep. Phys.* **67**(3), 872 (2015)
- [6] J. D. Vergados, H. Ejiri, and F. Simkovic, *Rep. Prog. Phys.* **75**, 106301 (2012)
- [7] J. Engel and J. Menéndez, *Rep. Prog. Phys.* **80**, 046301 (2017)
- [8] J. M. Yao, J. Meng, Y. F. Niu *et al.*, *Prog. Part. Nucl. Phys.* **126**, 103965 (2022)
- [9] G. Pantis, F. Simkovic, J. D. Vergados *et al.*, *Phys. Rev. C* **53**, 695 (1996)
- [10] V.A. Rodin, A. Faessler, F. Simkovic *et al.*, *Nucl. Phys. A* **766**, 107 (2006)
- [11] F. Simkovic, G. Pantis, J. D. Vergados *et al.*, *Phys. Rev. C* **60**, 055502 (1999)
- [12] M. Kortelainen, and J. Suhonen, *Phys. Rev. C* **76**, 024315 (2007)
- [13] J. Suhonen and M. Kortelainen, *In. J. Mod. Phys. E* **17**, 1 (2008)
- [14] D. L. Fang, A. Faessler, V. Rodin *et al.*, *Phys. Rev. C* **83**, 034320 (2011)
- [15] F. Simkovic, V. Rodin, A. Faessler *et al.*, *Phys. Rev. C* **87**(4), 045501 (2013)
- [16] D. L. Fang, A. Faessler, and F. Simkovic, *Phys. Rev. C* **97**(4), 045503 (2018)
- [17] J. Terasaki, *Phys. Rev. C* **86**, 021301(R) (2012)
- [18] J. Terasaki, *Phys. Rev. C* **91**, 034318 (2015)
- [19] J. Terasaki and Y. Iwata, *Phys. Rev. C* **100**, 034325 (2019)
- [20] J. Terasaki, *Phys. Rev. C* **102**, 044303 (2020)
- [21] W.L. Lv, Y.F. Niu, D.L. Fang *et al.*, *Phys. Rev. C* **105**, 044331 (2022)
- [22] N. Papara, A. Ravlic, and N. Paar, *Phys. Rev. C* **105**, 064315 (2022)
- [23] W. L. Lv, Y. F. Niu, D. L. Fang *et al.*, *Phys. Rev. C* **108**, L051304 (2023)
- [24] M. T. Mustonen and J. Engel, *Phys. Rev. C* **87**(6), 064302 (2013)
- [25] D. Navas-Nicolás and P. Sarriguren, *Phys. Rev. C* **91**, 024317 (2015)
- [26] N. Hinohara and J. Engel, *Phys. Rev. C* **105**, 044314 (2022)
- [27] T. Otsuka, T. Suzuki, R. Fujimoto *et al.*, *Phys. Rev. Lett.* **95**, 232502 (2005)
- [28] T. Otsuka, T. Matsuo, and D. Abe, *Phys. Rev. Lett.* **97**, 162501 (2006)
- [29] G. Colò, H. Sagawa, S. Fracasso *et al.*, *Phys. Lett. B* **646**, 227 (2007)
- [30] D. M. Brink and Fl. Stancu, *Phys. Rev. C* **75**, 064311 (2007)
- [31] C. L. Bai, H. Sagawa, H. Q. Zhang *et al.*, *Phys. Lett. B* **675**, 28 (2009)
- [32] C. L. Bai, H. Q. Zhang, X. Z. Zhang *et al.*, *Phys. Rev. C* **79**, 041301(R) (2009)
- [33] L.G. Cao, G. Colò, H. Sagawa *et al.*, *Phys. Rev. C* **80**, 064304 (2009)
- [34] C. L. Bai, H. Q. Zhang, X. Z. Zhang *et al.*, *Chin. Phys. Lett.* **27**, 102101 (2010)
- [35] C. L. Bai, H. Q. Zhang, H. Sagawa *et al.*, *Phys. Rev. Lett.* **105**, 072501 (2010)
- [36] F. Minato and C. L. Bai, *Phys. Rev. Lett.* **110**, 122501 (2013)
- [37] C. L. Bai, D. L. Fang, and H. Q. Zhang, *Chin. Phys. C* **46**, 114104 (2022)
- [38] M. Doi, T. Kotani, and E. Takasugi, *Prog. Theor. Phys. Suppl.* **83**, 1 (1985)
- [39] qR. A. Sen'kov and M. Horoi, *Phys. Rev. C* **88**, 064312 (2013)
- [40] F. Simkovic, L. Pacearescu, and A. Faessler, *Nucl. Phys. A* **733**, 321 (2004)
- [41] P. Ring and P. Schuck, *The Nuclear Many-Body Problem*, (Springer-Verlag)
- [42] J. Dobaczewski, H. Flocard, and J. Treiner, *Nucl. Phys. A* **422**, 103 (1984)
- [43] J. Terasaki, J. Engel, M. Bender *et al.*, *Phys. Rev. C* **71**, 034310 (2005)
- [44] T. H. R. Skyrme, *Philos. Mag* **1**, 1043 (1956)
- [45] T. H. R. Skyrme, *Nucl. Phys.* **9**, 615 (1959)
- [46] M. Agostini, A. M. Bakalyarov, M. Balata *et al.*, *Science*. **365**, 6460 (2019)
- [47] B. T. Zhang, J. Z. Wang, L. T. Yang *et al.*, *Chin. Phys. C*. **48**, 103001 (2024)
- [48] X. Cao, Y. Chang, K. Chen *et al.*, *NvDEx-100 Conceptual Design Report*, (2023), arXiv: 2304.08362
- [49] S. Abe, S. Asami, M. Eizuka *et al.*, *Phys. Rev. Lett.* **130**, 051801 (2023)
- [50] K. X. Ni, Y. H. Lai, A. Abdukerim *et al.*, *Chin. Phys. C*. **43**, 11 (2019)
- [51] G. Anton, I. Badhrees, P. S. Barbeau *et al.*, *Phys. Rev. Lett.* **123**, 161802 (2019)
- [52] P. Novella *et al.* (The NEXT Collaboration), *JHEP* **2019**, 51 (2019)
- [53] The CUORE Collaboration, *Nature*. **604**, 53 (2022)
- [54] N. Van Giai and H. Sagawa, *Phys. Lett. B* **106**, 379 (1981)
- [55] C. L. Bai, H. Q. Zhang, H. Sagawa *et al.*, *Phys. Rev. C* **83**, 054316 (2011)
- [56] T. Wakasa, M. Okamoto, M. Dozono *et al.*, *Phys. Rev. C* **85**, 064606 (2012)
- [57] T. Wakasa, H. Sakai, H. Okamura *et al.*, *Phys. Rev. C* **55**, 2909 (1997)
- [58] H. Akimune, I. Daito, Y. Fujita *et al.*, *Phys. Rev. C*. **52**, 604 (1995)
- [59] M. J. Yang, C. L. Bai, H. Sagawa *et al.*, *Phys. Rev. C* **103**, 054308 (2021)
- [60] M. J. Yang, C. L. Bai, H. Sagawa *et al.*, *Phys. Rev. C* **106**, 014319 (2022)
- [61] V. Rodin and A. Faessler, *Phys. Rev. C* **84**, 014322 (2011)
- [62] J. M. Yao, L. S. Song, K. Hagino *et al.*, *Phys. Rev. C* **91**(2), 024316 (2015)
- [63] A. S. Barabash, *Phys. Rev. C* **81**, 035501 (2010)
- [64] O. Civitarese, A. Faessler, and T. Tomoda, *Phys. Lett. B* **194**, 11 (1987)
- [65] M. S. Yousef, V. Rodin, A. Faessler *et al.*, *Phys. Rev. C* **79**, 014314 (2009)
- [66] D. L. Fang, *Chin. Phys. C* **48**(3), 034101 (2024)
- [67] O. Azzolini, J. W. Beeman, F. Bellini *et al.*, *Phys. Rev. Lett.* **123**, 262501 (2019)
- [68] A. Gando *et al.* (KamLAND-Zen), *Phys. Rev. Lett.* **122**(19), 192501 (2019)
- [69] R. Madey, B. S. Flanders, B. D. Anderson *et al.*, *Phys. Rev. C* **40**, 540 (1989)
- [70] P. Puppe, D. Frekers, T. Adachi *et al.*, *Phys. Rev. C* **84**, 051305 (1989)